Synthesis of Zinc-Copper-Iron(II, III) Oxide Nanocomposites and their Photocatalytic Efficiency for Crystal Violet Degradation

Sajid M. Mansoori[1*], Ramesh S. Yamgar[2] and Shreemant V. Rathod[3]
[1]Department of Chemistry, Mithibai College, Vile Parle (West), Mumbai-400 056, Maharashtra, India
[2]Department of Chemistry, Patkar College, Goregaon (West), Mumbai-400 062, Maharashtra, India
[3]Department of Chemistry, Bhavan's Hazarimal Somani College, K.M. Munshi Marge, Chowpatty-400 007, Mumbai, Maharashtra, India
[*]Corresponding author (e-mail: mohd.mansoori@mithibai.ac.in)

The synthesis, characterization, and application of metal oxide nanocomposites have received increasing interest in the field of nanoscience and technology with several possible opportunities. Nanocomposites containing two or more dissimilar band gaps semiconductors provide exceptional properties to photocatalysts. A simple chemical co-precipitation method was employed to synthesize ZnO:CuO:Fe_2O_3 mixed metal oxide nanocomposites followed by calcination at 500^0C. The prepared nanocomposites were characterized by XRD, FTIR, SEM, and TEM. The FTIR and XRD spectra confirmed the characteristic vibrations of ferrite atoms along with Cu-O and Zn-O vibrations. The crystallite particle size calculated by Debye Scherrer formula matched the size obtained by SEM and TEM images. The photocatalytic efficiency of the ZnO:CuO:Fe_2O_3 nanocomposites was assessed using crystal violet dye in the presence of sunlight. Variation in the concentration of Cu with respect to zinc in the nanocomposites enhanced photodegradation efficiency in this investigation. Our results indicated that the variation in the composition of ternary nanocomposite catalysts influence the competence for dye removal from waste water.

Key words: Nanocomposites; degradation; crystal violet; waste water

Received: April 2020; Accepted: September 2020

Leather, textile, paint, cosmetic, and pharmaceutical industries discharge partially treated and/or generate waste into land and water. This is polluting the local environment and spreading many diseases like allergic contact dermatitis, increased heart rate, vomiting, cyanosis, tissue necrosis, tumor, and enzyme disorders (1, 2).

Crystal violet (CV) dye provides a deep violet color to paint and printing ink in the textile processing industry. CV has been reported as an obstinate dye molecule that remains in the environment for a long period and carries toxic effects in the environment. The preceding account of CV disguises that this dye has now become one of the most argued and provocative compounds due to its damaging effects on the environment and severe health hazards mounted on living organisms. It also acts as a mitotic poison, a cancer-causing agent, and a cogent clastogen stimulating tumor growth in some species of fishes. Hence, for the degradation and detoxification of waste water, a persistent and effective treatment technique should be employed. Therefore, there is an exigent requirement to develop an environment friendly and cost effective process for the definite degradation and detoxification of CV for environmental welfare (3).

Numerous methods have been reported for effective elimination of CV dye from contaminated water (4). Amongst them, adsorption and photocatalysis played a very significant role in water treatment. The key challenges in the adsorption process is restoration of the adsorbents and stowage of toxic sludge. In recent years, toxic effluents have been eliminated from waste water by various types of photocatalysts (9-10). Water purification via semiconductor photocatalysis is an environmentally friendly and inexhaustible process, which converts dyes into gaseous products and do not pile up toxic sludge (11-12). A semiconductor photocatalyst absorbs photons with energy higher than its bandgap, causing electrons to jump into the conduction band and leaving holes in the valence band. These holes and electrons are powerful oxidants and reductants, and decontaminate organic and inorganic pollutants present in water, respectively. The high band gap, rapid electron-hole recombination, and weak semiconductor-pollutant interaction are the important challenges need to overcome for the effective harvesting of solar energy for different applications (13-14).

Hematite (α-Fe_2O_3) and ZnO are n-type semiconductors with energy band gaps of 3.37 eV and 2.2 eV, respectively (15-16). While CuO is a p-type semiconductor with energy band gap of 1.2 eV (17-18). Compared to other nano-sized semiconducting materials, ZnO is low cost, environmentally stable, and has received much attention in the degradation of environmental pollutants (19-20). ZnO has been used

for degradation of organic dyes, such as methyl orange (21), crystal violet (22-23), Rhodamine B (24), and methylene blue (25-26). ZnO/CuOcombined metal oxide semiconductors have been found to show higher photocatalytic activity under both UV and visible light irradiation than either pure ZnO or CuO (27-30). The coupled semiconductor materials have two types of energy-level systems, which play significant roles in realizing charge separation. Coupling of different semiconductor oxides can reduce the band gap, spreading the absorbance range to visible region, leading to electron–hole pair separation under irradiation, and subsequently succeeding a higher photocatalytic activity, due to synergetic effects (31–33). These systems also possess greater degradation of organic dyes. ZnO/SnO_2 (35), CuO–TiO_2 (36), Cu_2O/ZnO (35), Ag–ZnO (36), and ZnO/CuO (33, 37) are the types of coupled semiconductors synthesized successfully. Well-matched band edges of both p-type CuO and n-type ZnO in CuO-ZnO nanocomposites are appropriate to encourage the irreversible transfer of charge carriers from one semiconductor to another, thus suppressing recombination. ZnO coupled with CuO is used for various applications such as conductivity studies, photocatalytic activity, magnetic properties, and gas sensors. The presence of CuO along with ZnO can improve photocatalytic activity and increase spectral response, thus attracts significant interest, since the surface modification of semiconductor oxides with metals such as copper (Cu) or iron (Fe), an interfacial charge transfer mechanism, improves the photocatalytic activity against organic compounds (38-41). Therefore, the incorporation of Fe_2O_3/Fe_3O_4 nanoparticles into CuO:ZnO nanocomposites to form ternary Fe_2O_3/Fe_3O_4:CuO: ZnO nanocomposites could provide promising catalysts.

MATERIALS AND METHODS

Materials: Ferrous ammonium(II) sulfate hexahydrate $(NH_4)_2Fe(SO_4)_2{\cdot}6H_2O$, cupric nitrate trihydrate $(Cu(NO_3)_2.3H_2O$, 99.5%), zinc sulfate heptahydrate ($ZnSO_4{\cdot}7H_2O$, 99%), sodium hydroxide (NaOH), ethanol, and crystal violet were sourced from S.D. Fine Chem limited. All chemical reagents were of analytical grade and used without further purification.

Synthesis of ZnO:CuO:Fe_2O_3 Nanocomposites

ZnO:CuO:Fe_2O_3 nanocomposites were synthesized by a co-precipitation method from $Cu(NO_3)_2.3H_2O$, $ZnSO_4.7H_2O$, and $Fe(NH_4)SO_4.7H_2O$ dissolved in deionized water with 1:1:4, 3:1:4, and 1:3:4 ratios of CuO, ZnO, and Fe_2O_3, respectively. The metal ions were precipitated by adding 4N NaOH. The precipitates were filtered, washed several times with distilled water, and dried at 110^0C for 24 hours in an electric oven. The dried samples were calcined in a tube furnace at 500^0C in air for 6 hours (11, 13, 14).

Structural Characterization

A UV-Vis spectrophotometer (Systronic UV-2203) ran in the range of 300–800 nm was employed to measure the optical absorption spectrum. Fluorescence spectra of the prepared nanocomposites were recorded using Shimadzu RF-5301. Schimadzu XRD-7000 was used to record X-ray diffraction patterns, using CuKα, wavelength of radiation (λ = 0.15406 nm) in the range of 2theta 10 nm to 80 nm. A scanning electron microscope operated at 10.0 kV with energy dispersive X-Ray analysis (JEOL-JSM-6360A) estimated the particle size and elemental analysis of the prepared nanocomposites. Debye-Scherer's formula was employed to calculate the size of crystalline particles (18).

$$\text{Average particle size (D)} = \frac{0.9\lambda}{\beta cos\theta}$$

Where,

D = crystalline particle size

λ = wavelength of X-ray

β= diffraction peak broadening

θ = angle of diffraction

FTIR analyses were carried out using Perkin Elmer RFPC-5301 in the range of 500-4000 cm^{-1} in a KBr matrix. PHILIPS-CM 200 TEM was employed to observe the morphologies of the prepared nanocomposites.

Photocatalytic Activity Studies

The photocatalytic degradation of crystal violet was performed in a 250 cm^3 conical flask using synthesized ZnO:CuO:Fe_2O_3 as photocatalyst under sunlight for various time intervals. 10 mg of synthesized ZnO:CuO:Fe_2O_3 nanocomposite powder was equilibrated with 50 cm^3 of 10 ppm CV dye solution by shaking on a shaker for 30 min, before exposing to sunlight. At regular time intervals, the photocatalytic decomposition of CV was examine using a UV–visible spectrophotometer (Systronic UV-2203) at the wavelength of 595 nm.

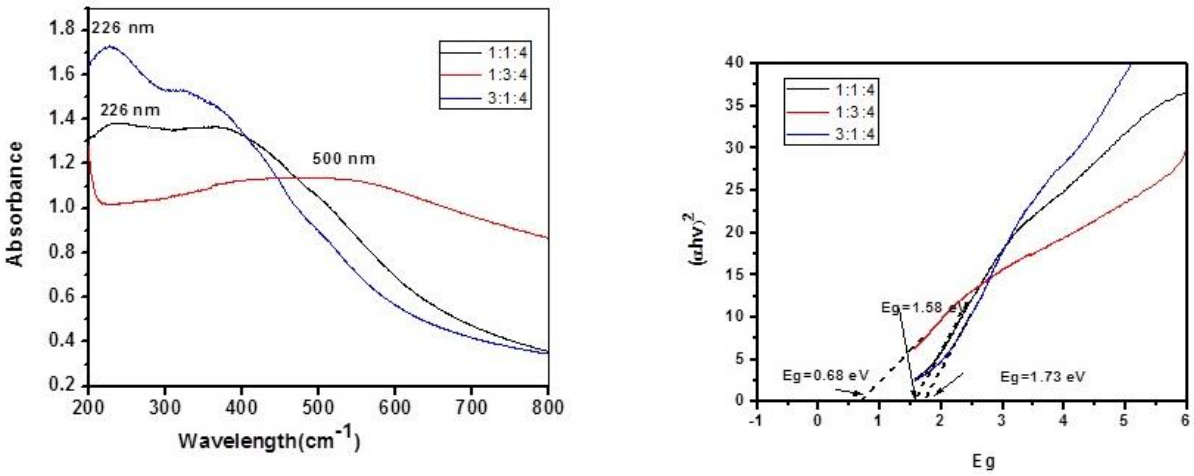

(a) (b)

Figure 1. (a) U.V absorption spectra and (b) binding energy curves of ZnO:CuO:Fe_2O_3 nanocomposites

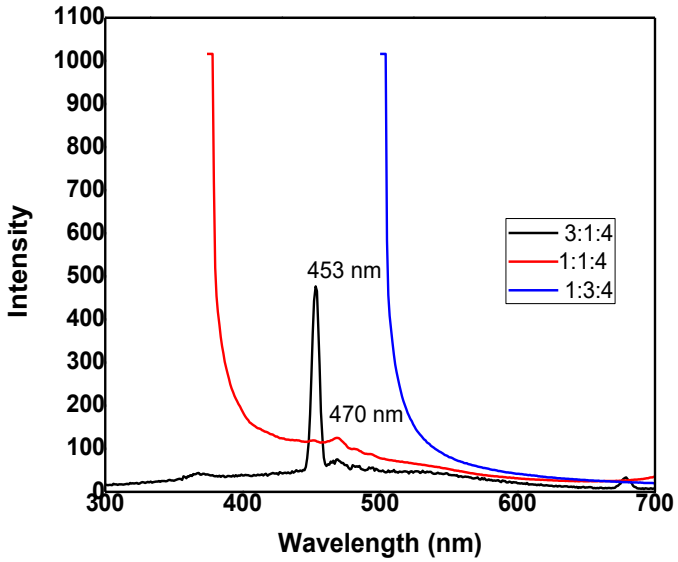

Figure 2. Fluorescence spectra of ZnO:CuO:Fe_2O_3 nanocomposites

RESULTS AND DISCUSSION

The ZnO:CuO:Fe_2O_3 nanocomposite with 1:3:4 ratio showed strong visible light absorption at 500 nm, while the ratios of 1:1:4 and 3:1:4 showed strong absorption in the UV region at 226 nm. Therefore, it was expected that the ZnO:CuO:Fe_2O_3 nanocomposite with 1:3:4 ratio possessed higher photocatalytic activity in the visible region. The higher molar ratio of CuO with respect to ZnO decreased the binding energy of the ZnO:CuO:Fe_2O_3 nanocomposite with 1:3:4 ratio to 0.68 eV, which was much lower than the other ratios, i.e. 1.58 eV and 1.73 eV for 1:1:4 and 3:1:4 ratios, respectively. Therefore, it was expected that the ZnO:CuO:Fe_2O_3 nanocomposite with 1:3:4 ratio possessed comparatively good semiconductor properties.

3:1:4 ratio showed fluorescence at 453 nm and 1:1:4 showed very little florescence at 470 nm, while 1:3:4 did not show any fluorescence. This indicated that degradation of CV using the ZnO:CuO:Fe_2O_3 nanocomposite of 1:3:4 ratio was completely due to photocatalytic degradation.

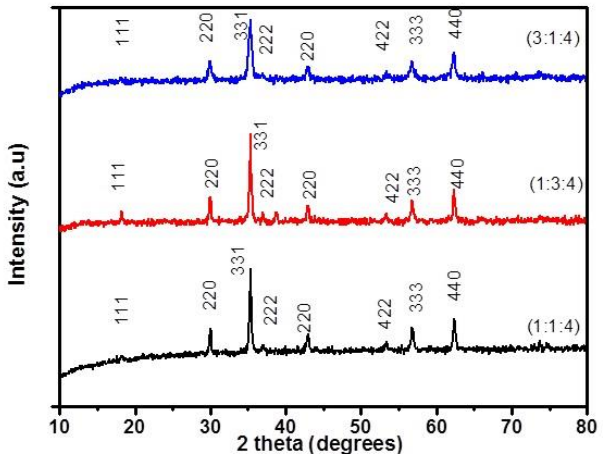

Figure 3. XRD spectra of ZnO:CuO:Fe_2O_3 nanocomposites

X-Ray diffraction studies showed the major diffraction peaks were between 15° and 65° (2θ). The diffraction peaks at 2θ values of 29.96°, 35.31°, 56.75°, and 62.30° corresponded to (220), (311), (222), (220), (333), and (440) planes of α-Fe_2O_3 nanoparticles (JCPDS 36-1451). The peak at 2θ = 29.96° was of (220) plane of Fe_3O_4. Hexagonal wurtzite structure of ZnO nanoparticle belonged to JCPDS data card No. 79-2205. The XRD pattern of the nanocomposites showed well developed peaks at 2θ = 18.23°, 38.71°, 42.9°, 53.3°, and 59.36° due to (1 1 0), (1 1 1), (1 1 1), (1 1 2), (2 0 2), (1 1 2), (0 2 0), (2 0 2), (1 1 3), and (0 2 2) planes, respectively, which confirmed the mono-clinic structure of CuO (JCPDS data card No. 89-2529). The peaks at 2θ = 18.2° assigned to (200) planes of CuO were observed to increase in intensity with the content of CuO, and the absence of other copper peaks in the XRD spectra confirmed that air oxidation occurred upon annealing at 500ºC. This suggested that oxides combined through inter grain coupling instead of intra granular coupling (37-41).

FTIR Spectra

The transmittance spectra of the ZnO:CuO:Fe_2O_3 nanocomposites are presented in Fig. 4. A broad peak around 550 cm^{-1} in the FTIR spectra corresponded to vibrational mode of M-O at tetrahedral site (19–21). Overlapping of Fe–O, Cu–O, and Zn–O stretching vibrations occurred between 400–800 cm^{-1}. According to related studies (37–39), the characteristic peaks of Fe–O in Fe_3O_4 were at 375 and 570 cm^{-1}, while the Cu–O stretching band in the monoclinic phase and the Zn–O stretching band were observed in 430–610 and 400–660 cm^{-1} regions, respectively. 1114-1128 cm^{-1} corresponded to the Cu-O stretching vibration (1000-1250 cm^{-1}). A peak at 1435 cm^{-1} was due to the C=O stretching vibration (31).

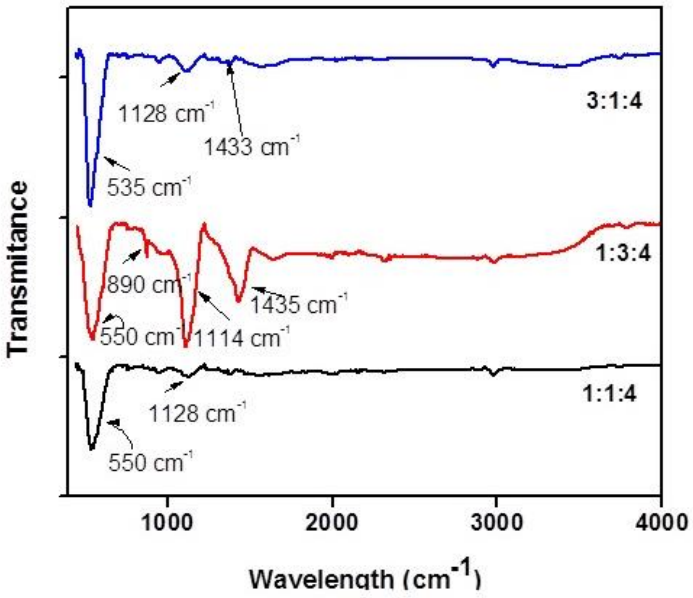

Figure 4. FTIR spectra of ZnO:CuO:Fe_2O_3 nanocomposites

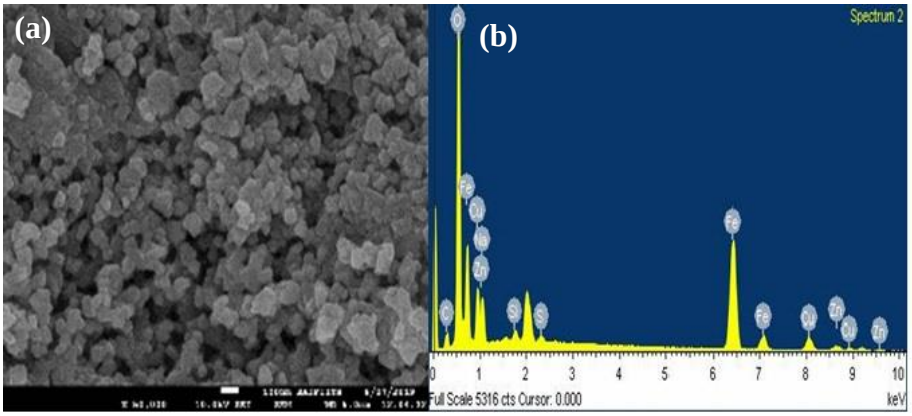

Figure 5a. FESEM of CuO:ZnO:Fe_2O_3 nanocomposite
Figure 5b. EDX of CuO:ZnO:Fe_2O_3 nanocomposite

SEM and EDX

The aggregated morphology of the nanocomposites has the mixture of nanoparticles with grain size around 10 to 40 nm, as shown in Fig. 5a. However, EDX spectra (Fig. 5b) confirmed the presence of the expected chemical elements in the samples. The prepared ZnO:CuO:Fe_2O_3 nanocomposites were in agreement with the EDX and XRD results.

TEM

Transmission electron microscopy studies of the ZnO:CuO:Fe_2O_3 nanocomposites showed rod-like structure of CuO, spherical Fe_2O_3, and wurtzite shape of ZnO, as shown in the TEM images in Fig. 6.

Photo Catalytic Activity

In this study, ZnO:CuO:Fe_2O_3 nanocomposites with different molar ratios were used for degradation reaction of CV. Photocatalytic efficiency increased as the molar ratio of CuO to ZnO increased from 1:1 to 1:3 in presence of visible light. Maximum degradation efficiency was 91.67% for 1:3:4 ratio of ZnO:CuO:Fe_2O_3, 80.15% for 1:1:4 ratio, and 56.11% for 3:1:4 ratio at 180 minutes, as shown in Fig. 7. Thus, the present study on degradation of crystal violet using ZnO:CuO:Fe_2O_3 ternary nanocomposites confirmed that the increase in ratio of CuO to ZnO favors charge separation, hence degradation was better than the other ratios where ZnO percentage was higher than CuO.

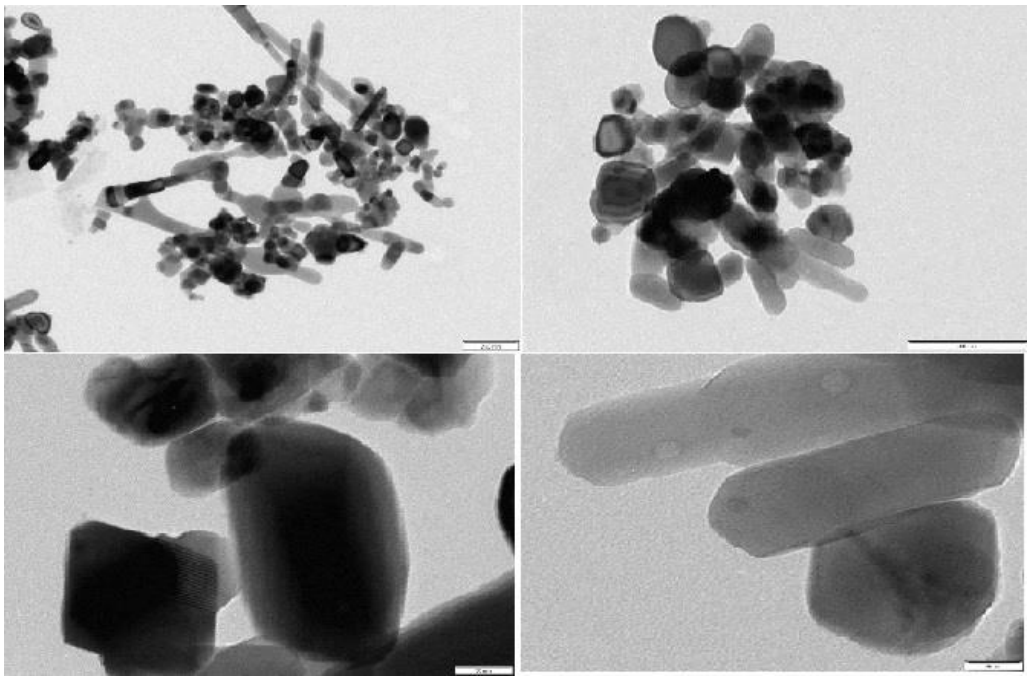

Figure 6. TEM images of the ZnO:CuO:Fe_2O_3 composite.

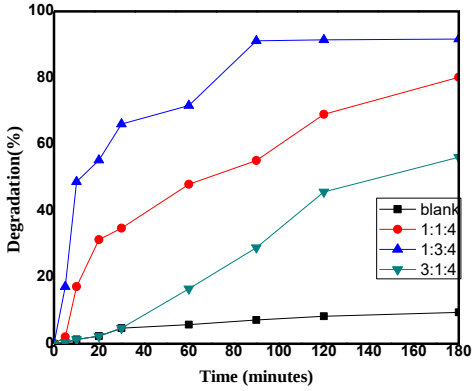

Figure 7. Degradation of crystal violet dye as function of time using different ratios of nanocomposites under visible light irradiation

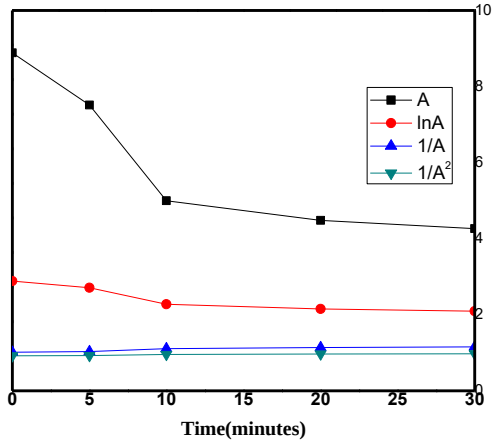

Figure 8. Plot of order of reaction for degradation of crystal violet using 1:3:4 nanocomposite

As shown in Fig. 8, the linearity of the plot shows that the degradation reaction of CV dye using the CuO:ZnO:Fe_2O_3 nanocomposite of 1:3:4 ratio as catalyst followed second order kinetics (R^2= 0.9238, k = 0.0345).

Above results concluded that the variation of CuO to ZnO in nanocomposites has great impact on photocatalytic activity of crystal violet. The CuO:ZnO:Fe_2O_3 nanocomposite of 1:3:4 ratio resulted in restrained recombination of photo-generated electrons and holes.

To understand the mechanism of the photocatalysis, various factors should be considered, such as the generation, trapping, and recombination of charge carriers, average crystallite size, band gap, specific surface area, and defect or localized states (42). These factors are related to the composition of the catalyst and the nature of target pollutants. Based on related literature reports (14, 39, 41, 44), degradation of CV by CuO:ZnO:Fe_2O_3 nanocomposites under visible light can be explained by the possible mechanism shown in Fig. 9.

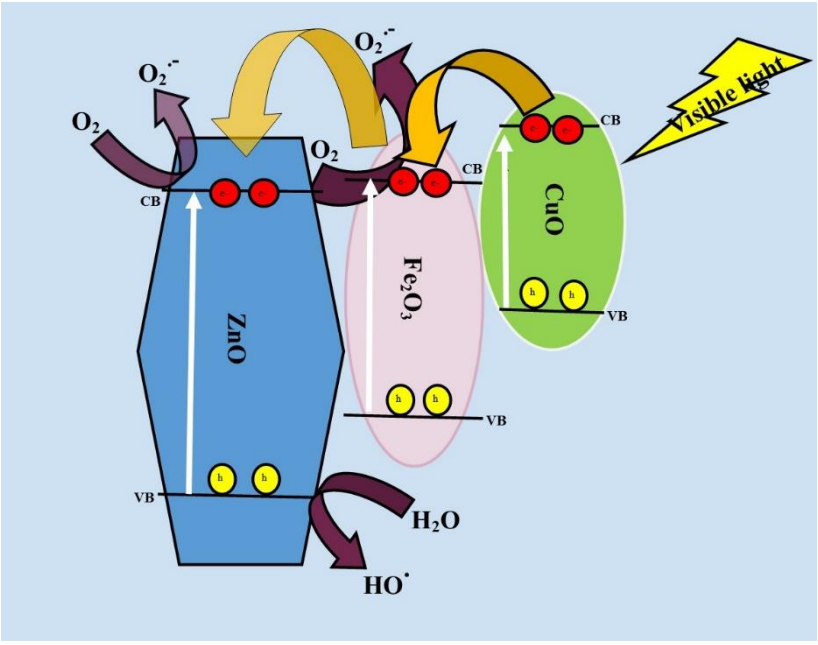

Figure 9. Proposed mechanism for degradation of CV dye using CuO:ZnO:Fe_2O_3 nanocomposites

Under visible light, ZnO is not active, however CuO easily get activated and create electron-hole pairs (42, 45, 46). The photo-generated electrons (e^-) can be transferred from the CB of CuO to the CB of Fe_2O_3, and then to the CB of ZnO. The photocatalytic efficiency is enhanced by $O_2\bullet^-$, which could be generated due the interaction of O_2 molecules with electrons. In addition, Fe^{3+} react with photo-generated electrons and produce Fe^{2+} ions. Furthermore, surface-bound and/or Fe^{2+} ions react with dissolved oxygen to generate superoxide radicals. The contribution of electrons in the formation of Fe^{2+} ions most likely decreases the probability of the recombination of electron-hole and increase hydroxyl radical formation (47). Moreover, oxidation of water molecules by the holes generates HO●. Thus, HO● and $O_2\bullet$- are generated due to electron and hole (e^- /h^+) transfers (48). These molecules are strongly capable of degrading CV molecules by bonds breakdown and finally cause mineralization. In addition, CV can be eliminated directly from the solution by oxidation using h^+ at the CuO/Fe_2O_3/ZnO surface (47).

CONCLUSION

A simple co-precipitation method was employed to prepare ZnO:CuO:Fe_2O_3 nanocomposites. The FTIR spectra of the samples showed the presence functional groups attributable to metal oxides. The XRD results revealed that the prepared samples were nanosize and strong peaks showed the presence of ZnO:CuO:Fe_2O_3 nanocomposites. TEM images of the nanocomposites showed rod-like, spherical, and wurtzite shape of the crystals of CuO, Fe_2O_3 and ZnO, respectively. The photocatalytic activity of the nanocomposite with molar ratio of 1:3:4 of ZnO:CuO:Fe_2O_3 possessed good photo response under visible light irradiation. The improved photocatalytic activity of the prepared nanocomposite might be due to the increased percentage of CuO with respect to ZnO in the nanocomposite. Further studies could be done in order to get better understanding of the role of variation of metal oxides in nanocomposites for degradation of dyes.

ACKNOWLEDGMENTS

The authors acknowledge IIT-Bombay for SEM/EDAX/TEM analyses and University of Mumbai for fluorescence spectra, FTIR and XRD analyses.

REFERENCES

1. Gordon, P. F. and Gregory, P. (1983) Organic Chemistry in Colour. *Springer Verlag Berlin Heidelberg, New York*.

2. Chiron, S., Fernández-Alba, A. R., Rodr´ıguez, A., Garc´ıa-Calvo, E. (2000) *Wat. Res.*, **34(2)**, 366.

3. Ollis, D. F., Pelizzetti, E., Serpone, N., (1991) Photocatalyzed destruction of water contaminants, *Environ. Sci. Technol.*, **25**, 1523.

4. Hoffmann, M. R., Martin, S. T., Choi, W., Bahnemann, D. W. (1995) Environmental applications of semiconductor photocatalysis, *Chem. Rev.*, **95**, 69-96.

5. Ahmad A. Mohd, Setapar, S. H., Chuong, C. S., Khatoon A., Wani, W. A., Kumar, R., Rafatullah, M. (2015) Recent advances in new generation dye removal technologies: Novel search for approaches to reprocess wastewater. *RSC Adv*, **5**, 30801–30818.

6. Malato, S., Blanco, J., Herrmann, J. M. (Eds.) (1999) Solar Catalysis for Water Decontamination, *Catal. Today*, **54**, 2–3.

7. Chatterjee, D. and Dasgupta, S. (2005) Visible light induced photocatalytic degradation of organic pollutants, *J Photochem Photobiol C – Photochem Rev.*, **6**,186–205.

8. Chen, C., Ma, W., Zhao, J., (2010) Semiconductor-mediated photodegradation of pollutants under visible-light irradiation, *Chem. Soc. Rev*., **39**, 4206–4219.

9. Chakrabarti, S. and Dutta, B. K. (2004) Photocatalytic degradation of model textiles dyes in waste-water using ZnO as semiconductor catalyst, *J. Hazard Mater.*, **112(2)**, 69–278.

10. Mageshwari, K., et. al. (2015) Improved photocatalytic activity of ZnO coupled CuO nanocomposites synthesized by reflux condensation method, *J. Alloys Compd*., **625**, 362–370.

11. Zhang, Z., et. al. (2008) Cu-doped ZnO nanoneedles and nanonails: morphological evolution and physical properties; *J. Phys. Chem. C*., **112**(26), 9579–9585.

12. Chen, C., Ma, W., Zhao, J. (2010) Semiconductor-mediated photodegradation of pollutants under visible-light irradiation, *Chem. Soc. Rev.*, **39**, 4206–4219.

13. Habib, M. A., Ismail, I. M. I., Mahmood, A. J., Ullah, M. R. (2012) Photocatalytic decolourization of brilliant golden yellow in TiO_2 and ZnO suspensions, *J. Saudi Chem. Soc.*, **16**, 423–429.

14. Taufik, A., Saleh, R. (2017) Synthesis of iron (II, III) oxide/zinc oxide/copper (II) oxide (Fe_3O_4/ZnO/CuO) nanocomposites and their photosonocatalytic property for organic dye

removal, *J. Colloid Interface Sci.*, **491**, 27–36.

15. Quan, Z., et. al. (2010) Microstructures, surface bonding states and room temperature ferromagnetisms of $Zn_{0.95}Co_{0.05}O$ thin films doped with copper, *Appl. Surf. Sci.*, **256(11)**, 3669–3675.

16. Ashokkumar, M., Muthukumaran, S. (2014) $Zn_{0.96-x}Cu_{0.04}$ Fe_xO (($0 \leq x \geq 0.04$)) alloys–Optical and structural studies, *Superlatt. Microstruct*, **69**, 53–64.

17. Cai, Y., Fan, H., Xu, M., Li, Q. (2013) Rapid photocatalytic activity and honeycomb Ag/ZnO heterostructures via solution combustion synthesis, *Colloids Surf.*, A **436**, 787– 795.

18. Joshi, B. N., Yoon, H., Na, S., Choi, J. Y, Yoon, S. S. (2014) Enhanced photocatalytic performance of graphene–ZnO nanoplatelet composite thin films prepared by electrostatic spray deposition, *Ceram. Int.*, **40**, 3647–3654.

19. Linhua Xu, et. al., (2017) Improved photocatalytic activity of nanocrystalline ZnO by coupling with CuO, *Journal of Physics and Chemistry of Solids*, **106**, 29–36.

20. Lee, K. M., et. al. (2016) Recent developments of zinc oxide based photocatalyst in water treatment technology: A review, *Water Research*, **88**, 428-448.

21. Chen, et. al. (2017) Preparation of ZnO Photocatalyst for the Efficient and Rapid Photocatalytic Degradation of Azo Dyes, *Nanoscale Research Letters*, **12**:143.

22. Sadia Ameen, et. al. (2013) Rapid photocatalytic degradation of crystal violet dye over ZnO flower nanomaterials. *Materials Letters*, **96**, 228–232.

23. Habib, et. al., (2013) Photocatalytic decolorization of crystal violet in aqueous nano-ZnO suspension under visible light irradiation, *Journal Of Nanostructure in Chemistry*, **3**, 70.

24. Cai, X. Y., Liu, Y. J., Zeng, H., Cai, Y., Li, H., Zhang, F. & Wang, Y. D. (2012) Synthesis and characterisation of alkali metal (Mn, Fe) oxide–ZnO nanorod composites and their photocatalytic decolourization of rhodamine B under visible light, *Materials Technology*, **27(5)**, 380-387.

25. Sampa Chakrabarti (2004) Photocatalytic degradation of model textile dyes in wastewater using ZnO as semiconductor catalyst, *Journal of Hazardous Materials* B, **112**, 269–278.

26. Volkan Eskizeybeka, et. al. (2012) Preparation of the new polyaniline/ZnO nanocomposite and its photocatalytic activity for degradation of methylene blue and malachite green dyes under UV and natural sun lights irradiations, *Applied Catalysis B: Environmental*, **119-120**, 197– 206.

27. Yang, C., Cao, X., Wang, S., Zhang, L., Xiao, F., Su, X., Wang, J. (2015) Complex-directed hybridization of CuO/ZnO nanostructures and their gas sensing and photocatalytic properties, *Ceram. Int*., **41**, 1749–1756.

28. Zhang, Q., Zhang, K., Daguo Xu, Yang, G., Huang, H., Nie, F., Liu, C., Yang, S. (2014) Synthesis, Characterization, growth mechanisms, fundamental properties, and applications, *Prog. Mater. Sci.*, **60**, 208–337.

29. Ghosh, A., Mondal, A. (2016) Fabrication of stable, Fabrication of stable, efficient and recyclable p-CuO/n-ZnO thin film heterojunction for visible light driven photocatalytic degradation of organic dyes, *Mater. Lett*, **164**, 221–224.

30. Saravanan, R., Karthikeyan, S., Gupta, V. K., Sekaran, G., Narayanan, V., Stephen, A. (2013) Enhanced photocatalytic activity of ZnO/CuO nanocomposite for the degradation of textile dye on visible light illumination, *Mater. Sci. Eng., C*. **33**, 91–98.

31. Hernandez, A., Maya, L., Mora, E. S., Sanchez, E. M. (2007) Sol-gel synthesis, characterization and photocatalytic activity of mixed oxide ZnO-Fe2O3, *J. Sol-Gel Sci. Technol.*, **42**, 71–78.

32. Shen, S., Kronawitter, C., Kiriakidis, G. (2017) An overview of photocatalytic materials, *Journal of Materiomics doi: 10.1016/j.jmat.2016.12.004*.

33. Samad, A., Furukawa M., Katsumata H., Suzuki T., Kaneco, S. (2016) Photocatalytic oxidation and simultaneous removal of arsenite with CuO/ZnO photocatalyst, *J. Photochem. Photobiol*, A, **325**, 97–103.

34. Nejat Redwan Habib, *et. al.* (2018) Synthesis, characterization and photocatalytic activity of $Mn_2O_3/Al_2O_3/Fe_2O_3$ nanocomposite for degradation of malachite green, *Bull. Chem. Soc. Ethiop*, **32**, 1,101-109.

35. Kandjani, A. E.; Sabri, Y. M.; Periasamy, S. R.; Zohora, N.; Amin, M. H.; Nafady, A.; Bhargava, S. K. (2015) Controlling Core/Shell formation of nanocubic p-Cu_2O/n-ZnO toward enhanced photocatalytic performance, *Langmuir*, **31**, 10922−10930.

36. Liu, X., Li, W., Chen, N., Xing, X., Dong, C., Wang, Y. (2015) Ag–ZnO heterostructure nanoparticles with plasmon-enhanced catalytic degradation for Congo red under visible light, *RSC Adv.*, **5**, 34456–34465.

37. Chang, T., Li, Z., Yun, G., Jia, Y., Yang, H. (2013) Enhanced photocatalytic activity of ZnO/CuO Nanocomposites synthesized by hydrothermal method, *Nano-Micro Lett*, **5**, 163–168.

38. Susmita Das, Vimal Chandra Srivastava (2016) Hierarchical nanostructured ZnO-CuO nanocomposite and its photocatalytic activity *Journal of Nano Research*, **35**, 21–26.

39. Ardiansyah Taufik and Rosari Saleh (2017) Synergistic effect between ternary iron–zinc–copper mixed oxides and graphene for photocatalytic water decontamination, *Ceramics International*, **43**, 3510–3520.

40. Taufik, A., Tju, H., Saleh, R. (2016) Comparison of Catalytic Activities for Sonocatalytic, Photocatalytic and Sonophotocatalytic Degradation of Methylene Blue in the Presence of Magnetic Fe_3O_4/CuO/ZnO Nanocomposites, *Journal of Physics*: *19 Conference Series 710 012004.*

41. Alam, U., Khan, A., Bahnemann, D., Muneer, M. (2018) Synthesis of iron and copper cluster-grafted zinc oxide nanorod with enhanced visible-light-induced photocatalytic activity, *J. Colloid. Interface. Sci*., **509**, 68–72.

42. Wang, Y., Zhao, X., Cao, D., Wang, Y., Zhu, Y. (2017) Peroxymonosulfate enhanced visible light photocatalytic degradation bisphenol A by Single-Atom dispersed Ag mesoporous g-C_3N_4 hybrid, *Appl. Catal. B.*, **211**, 79–88.

43. Samuel Hong Shen Chan (2011) Recent developments of metal oxide semiconductors as photocatalysts in advanced oxidation processes (AOPs) for treatment of dye waste-water, *J. Chem. Technol. Biotechnol.*, **86**, 1130–1158.

44. Gupta, R., Eswar, N. K., Modak, J. M., Madras, G. (2018) Ag and CuO impregnated on Fe doped ZnO for bacterial inactivation under visible light, *Catal. Today*, **300**, 71–80.

45. Jing Liu, et. al. (2012) Nanostructures for enhanced photocatalytic property, *Journal of Colloid and Interface Science*, **384**, 1–9.

46. Pirhashemi, M., Habibi-Yangjeh, A., Rahim Pouran, S. (2018) Review on the criteria anticipated for the fabrication of highly efficient ZnO-based visible-light-driven photocatalysts, *J. Ind. Eng. Chem*, **62**, 1–25.

47. Sakine Shekoohiyan, et. al. (2020) A novel CuO/Fe_2O_3/ZnO composite for visible-light assisted photocatalytic oxidation of Bisphenol A: Kinetics, degradation pathways, and toxicity elimination, *Separation and Purification Technology*, **242**, 116821.